Cancer Nanotechnology

RESEARCH Open Access

HepG2 exosomes coated luteolin nanoparticles remodeling hepatic stellate cells and combination with sorafenib for the treatment of hepatocellular carcinoma

Shengjie Ye[1,2], Xier Pan[1,2], Linghui Zou[1,2], Shuting Ni[2], Lei Zhang[3*], Yanlong Hong[3*] and Kaili Hu[1,2*]

*Correspondence: zhanglei37@sina.com; hfuir@163.com; kaili-hu@163.com

[1] School of Pharmacy, Shanghai University of Traditional Chinese Medicine, Shanghai 201203, China
[2] Shanghai Frontiers Science Center of TCM Chemical Biology, Institute of Interdisciplinary Integrative Medicine Research, Shanghai University of Traditional Chinese Medicine, Shanghai 201203, China
[3] Shanghai Innovation Center of TCM Health Service, Shanghai University of Traditional Chinese Medicine, Shanghai 201203, China

Abstract

Background: Hepatocellular carcinoma (HCC) is a common malignant tumor with high mortality and recurrence rate. The efficacy of the first-line drug sorafenib is impeded by drug resistance, which is closely related to activated hepatic stellate cells (HSCs). The natural product luteolin is good at alleviating the activation of HSC. However, its clinical application is limited to poor solubility, bioavailability and lacking of HSCs targeting effects. This study aims to construct luteolin-loaded biomimetic nanoparticles based on HepG2 exosomes for targeting HSCs and enhancing the therapeutic effects of sorafenib on HCC.

Methods: The HepG2 exosomes extracted were identified by size distribution, Zeta potential and characteristic proteins. Luteolin-loaded polylactic acid-glycolic acid (PLGA) nanoparticles (Lut-NPs) were prepared and wrapped by HepG2 exosomes to form biomimetic nanoparticles (Exo-Lut-NPs). A HepG2 cell sorafenib-resistant model induced by LX2 cell conditioned medium (CM) was established to evaluate the effects of Exo-Lut-NPs on reversing sorafenib-resistant in vitro. And the combined therapeutic effects of Exo-Lut-NPs with sorafenib were evaluated on a HepG2/LX2 subcutaneous xenograft tumor model in vivo.

Results: The particle size, drug loading capacity and encapsulation efficiency of Exo-Lut-NPs were 165 ± 10 nm, 2.6 ± 0.2% and 56.9 ± 4.3%, respectively. The in vitro HepG2 sorafenib-resistant model was induced by the CM of LX2 cells, and the results showed that Exo-Lut-NPs partially reversed the sorafenib resistance of HepG2 cells by affecting the CM of LX2 cells. The combined therapy of Exo-Lut-NPs with sorafenib markedly suppressed tumor growth in a HepG2/LX2 subcutaneous xenograft tumor model.

Conclusions: This study suggests that the Exo-Lut-NP is a novel and promising biomimetic delivery system which can combine with sorafenib for HCC therapy.

Keywords: Biomimetic nanoparticles, Hepatic stellate cells, Luteolin, Sorafenib, Hepatocellular carcinoma

Introduction

Liver cancer is one of the most common cancers, with the third largest death toll (8.3%) and the second highest mortality (90%) among all cancer kinds all over the world (Grandhi et al. 2016; Xia et al. 2022; Sung et al. 2020). Hepatocellular carcinoma (HCC) is the most common type of liver cancer. Currently, treatments for HCC, including surgical resection, liver transplantation, radiotherapy, chemotherapy and targeted therapy, are selectively applied in the clinic (European association for the study of the liver, European organisation for research and treatment of cancer 2012). Sorafenib is a multikinase inhibitor with anti-angiogenesis effects and is the most popular first-line drug approved by the US Food and Drug Administration (FDA) for HCC treatment (Zhu et al. 2017; Wilhelm et al. 2004). However, the beneficiary population only accounts for 12% of HCC patients treated with sorafenib (Eisai and Co., INC 2018). Worse still, the long-term administration of sorafenib not only leads to the abnormal activation of signal transduction and transcriptional activation protein 3 (STAT3) and Wnt/β-catenin pathways but also promotes the process of epithelial-mesenchymal transformation (EMT), both of which rapidly cause drug resistance within 6 months for these beneficiaries (Xia et al. 2020; Qiu et al. 2019; Xu et al. 2020; Marcucci et al. 2016; Maheswaran and Rushbrook 2012). Aiming to overcome sorafenib resistance, previous studies have combined sorafenib with other chemotherapeutic drugs, such as irinotecan, oxaliplatin (Wang et al. 2015a), lenvatinib, 5-fluorouracil (Ma et al. 2020), doxorubicin (Abou-Alfa et al. 2010), gemcitabine (Liu et al. 2015), molecular-targeted drugs, such as cetuximab (Xue et al. 2016), erlotinib (Zhu et al. 2015), kupanici (Ye et al. 2019), and immunotherapeutic drugs, such as anti-PD-L1 monoclonal antibodies (Wang et al. 2015b). Yet, these strategies have still faced the challenge of slight efficacy (Tang et al. 2020).

The tumor microenvironment which comprises immune cells and stromal cells, is closely related to the development of HCC. Hepatic stellate cells (HSCs) are resident mesenchymal cells, accounting for about one-third of the nonparenchymal cells and 15% of the resident cells in the normal liver (Friedman 2008). Under physiological conditions, HSCs play a vital role in generating matrix components and regulating hepatic sinus blood flow and portal vein pressure (Li et al. 2012; Higashi et al. 2017; D'Ambrosio et al. 2011). While HSCs in the tumor microenvironment promote the proliferation, migration, and invasion of liver cancer cells by secreting growth factors and cytokines (Shiraha et al. 2020; Niu et al. 2021). Increasing evidence has demonstrated that the interaction between hepatoma cells and activated HSCs promotes the acquisition of drug resistance to sorafenib (Azzariti et al. 2016; Seitz et al. 2020; Ruan et al. 2020). Thus, therapeutic targeting of HSCs has emerged as a prospective strategy for HCC treatment by inhibiting HSC activation and reversing HSCs to a quiescent state.

Luteolin is a natural flavonoid compound that is derived from broccoli, pepper, thyme, and celery (Lee and Kwon 2019). Studies have demonstrated that luteolin can not only significantly inhibit liver cancer cells by eliciting apoptosis, autophagy, and endoplasmic reticulum stress but also thwart the proliferation of activated HSC and collagen synthesis, thereby regarded as a promising candidate for HCC treatment (Lee and Kwon 2019; Chang et al. 2014; Zou et al. 2020; Cummins et al. 2018). Unfortunately, the clinical therapeutic outcomes after oral administration of luteolin are still far from satisfactory due to its poor water-solubility and low bioavailability (Chakrabarti and Ray

2015). The encapsulation of luteolin into nanoparticles is a potential remedy for handling flaws in administration of the free drug. The FDA has approved PLGA copolymers for pharmaceutical application due to their sound biocompatibility and biodegradability. These copolymers have also been widely developed as nanodrug carriers to enhance the solubility and bioavailability of poorly water-soluble chemicals (Chen et al. 2019; Pinto et al. 2022). However, these polymer nanoparticles without any modification are usually cleared from the peripheral circulation before reaching the target position, leading to limited accumulation in the tumor area (Ruman et al. 2020). Inspired by this, targeted nanodelivery to liver tumor sites to increase the luteolin accumulation is further considered.

In recent years, cell-derived exosomes have been widely developed as targeting drug delivery carriers with the advantages of low immunogenicity and long half-life (Xin et al. 2014; Liu et al. 2019a; Pei et al. 2021; Li et al. 2020, 2022). The surface adhesion proteins that are naturally inherited from parent cells endow exosomes with organ tropism and protect them from phagocytosis by monocytes and macrophages. Liu et al. found tumor cell-derived exosome-coated PLGA nanoparticles exhibited superior homotypic targeting ability compared with those coated with tumor cell membranes in both vitro and in vivo models (Liu et al. 2019a). Pei et al. constructed M2 macrophages-derived exosome-coated PLGA nanoparticles for the targeted delivery of Dnmt3aos $^{\text{smart silencer}}$ to treat allergic asthma (Pei et al. 2021). Increasing evidence shows that exosomes play a vital role in the communication between hepatoma cells and HSCs, indicating that exosomes may be potential drug vectors with a specific cell-targeting ability in HCC therapy (Zhou et al. 2018). Previous studies demonstrated that exosomes secreted from hepatoma cells had excellent HSC-targeting capability (Zhou et al. 2018; Li et al. 2017; Luo et al. 2021; Wang et al. 2018a). Compared to normal liver cells, extracellular vesicles derived from various liver cancer cells exhibited better HSC targeting properties (Zhou et al. 2018). Therefore, PLGA nanoparticles coated with the hepatoma cell-derived exosome membrane may achieve the targeted delivery of luteolin to HSCs for HCC treatment by remodeling HSCs in the tumor microenvironment.

In this study, we constructed biomimetic nanoparticles named exosome-coated luteolin-loaded PLGA nanoparticles (Exo-Lut-NPs) to target HSCs and combined Exo-Lut-NPs with sorafenib for HCC treatment. The exosomes isolated from HepG2 cells (a human HCC cell line) with the method of differential centrifugation were characterized by the particle size, Zeta potential, morphology, and characteristic proteins including heat shock protein 70 (HSP70), CD63, TSG101, CD9, and CD81. The luteolin-loaded PLGA nanoparticles without exosome coating (Lut-NPs) and Exo-Lut-NPs were also characterized by particle size, Zeta potential, drug loading capacity (DLC), encapsulation efficiency (EE), morphology and in vitro release profiles under pH 7.4 and pH 5.5. The HSC targeting effects of nanoparticles were investigated on LX2 cells by synthesized DiD loaded nanoparticles with or without exosome coating (DiD-NPs and Exo-DiD-NPs). Moreover, we evaluated the indirect anti-tumor effects of Exo-Lut-NPs on LX2 cell conditioned medium-induced HepG2 cell sorafenib-resistant model in vitro and investigated the combined therapeutic effects of Exo-Lut-NPs and sorafenib on an HCC subcutaneous xenograft mouse model.

Materials and methods

Cells and animals

HepG2 and LX2 cells were kind gifts from the Department of Hepatology, Shuguang Hospital, Shanghai University of Traditional Chinese Medicine (Shanghai, China). The Additional file 1 provided the identification results of short tandem repeat (STR) for HepG2 cells and LX2 cells. The cells were cultured with a complete medium composed of Dulbecco's modified Eagle's medium (DMEM; Meilunbio, China) supplemented with 10% (v/v) fetal bovine serum (FBS; Gemini, USA) and 1% penicillin/streptomycin (Basalmedia, China) at 37 °C in 5% CO_2. Both HepG2 and LX2 cells were detached using 0.25% and passaged twice per week at a subcultivation ratio of 1:3. The medium was renewed every 2–3 days. Twenty male Balb/c nude mice (4 weeks) were purchased from Charles River (Beijing, China) and bred in specific pathogen-free facilities. The experimental procedures were specifically approved by the Institutional Animal Care and Use Committee of Shanghai University of Traditional Chinese Medicine (IACUC No: PZSHUTCM220124025). All animal experiments were performed according to the animal welfare guidelines and the "3R" principle (reduction, replacement and refinement).

Isolation and characterization of HepG2 exosomes

Exosome isolation was performed with the differential centrifugation method as reported previously with some modifications (Pei et al. 2021; Wang et al. 2020). Briefly, after HepG2 cells were cultured in serum-free DMEM medium for 2 days, the medium was collected for exosome isolation, and then replaced with fresh DMEM medium for another 2 days before collecting the medium again. The medium was centrifuged at 300 g for 10 min, 2000 g for 10 min to remove dead cells, and 10,000 g for 30 min to discard cell debris, followed by filtration on a 200-nm syringe filter. The filtrate was concentrated by ultrafiltration (100 kDa, PES membrane, Sartorius) and then ultracentrifuged at 126,100 g for 2 h using SW 70 Ti rotor (Beckman coulter, Atlanta, Georgia, USA). Finally, the pellet was resuspended in PBS (pH = 7.2–7.4) which was composed of 137 mM NaCl, 2.67 mM KCl, 10 mM Na_2HPO_4 and 2 mM KH_2PO_4, and stored at − 80℃ for further use (Wang et al. 2018b, 2020, 2022; Théry et al. 2006; Witwer et al. 2013; Wu et al. 2021).

The size distribution and the particle concentration of HepG2 exosomes were measured by qNano (iZON Science, Christchurch, New Zealand) and the Zeta potential was measured by Malvern laser particle size analyzer (Malvern Instruments, Malvern, UK). According to previous studies (Wang et al. 2018b; Lin et al. 2021; Kouwaki et al. 2016; Xiao et al. 2013), HepG2 exosomes expressed characteristic proteins, including HSP70, CD63, TSG101, CD9, CD81 which were identified by the western blotting method. HepG2 cells were used as the positive control and culture medium was used as the negative control. HepG2 cells and exosomes were lysed in RIPA buffer (P0013B, Beyotime, China) with a protease inhibitor cocktail (P1005, Beyotime Biotechnology, China), a phosphatase inhibitor cocktail (P1096, Beyotime Biotechnology, China) and PMSF solution (Beyotime Biotechnology, China). The protein content was measured by a BCA protein concentration determination kit (Thermo, USA) according to the manufacturer's instructions. Proteins were separated in 10% sodium dodecyl sulfate–polyacrylamide gel

electrophoresis (SDS-PAGE) and transferred to a PVDF membrane (Beyotime, China). The membrane was blocked in 5% skim milk for 90 min and then incubated with primary antibodies (anti-HSP70, CD63, TSG101, CD9, CD81 antibody; 1:1000; Abcam, Cambridge, MA) overnight. Then blots were incubated with HRP-conjugated secondary antibodies (anti-rabbit or anti-mouse antibody; 1:1000) for 2 h. The Gel imaging system (Tanon, China) was used for the imaging of the band ($n=3$).

The HepG2 exosomes were visualized with the JEM-F200 transmission electron microscopy (TEM; FEI, USA) by "negative staining" method. Briefly, the exosome sample was incubated for 3 min on top of carbon-coated 300-mesh copper grids at room temperature (RT). Then grids were fixed in 3% phosphotungstic acid solution for 3 min at RT and blotted dry with filter paper, followed by analysis with TEM ($n=3$).

Preparation of luteolin-loaded PLGA nanoparticles and biomimetic nanoparticles

The Lut-NPs were synthesized using a modified nanoprecipitation method (Zhang et al. 2018; Copp et al. 2014). The poly (dl-lactic-co-glycolic acid) (50:50 PLGA, 0.4 dl/g, Lactel Absorbable Polymers, USA) and luteolin (98% purity, Chengdu Herbpurify Co., Ltd., China) were initially dissolved in acetone. Then 0.5 mL of the solution was rapidly added to 1 mL of deionized water. The mixture was placed in a vacuum aspirator until the organic solvent was evaporated completely and the Lut-NPs (PLGA core) were acquired. To optimize the formulation, the effects of PLGA solution concentrations (5, 10 and 20 mg/mL) and luteolin/PLGA ratios (w/w: 5%, 4% and 3%) on four parameters, including the particle size, Zeta potential, DLC and EE were investigated. Subsequently, the Exo-Lut-NPs were fabricated by the extrusion method which was frequently used for the preparation of membrane-coating nanoparticles (Hu et al. 2011; Fang et al. 2014). Briefly, the HepG2 exosomes were mixed with Lut-NPs with the polymer/membrane protein ratio of 2:1 (w/w) (Zhang et al. 2018; Hu et al. 2011) and coextruded 7 times through a 200 nm polycarbonate membrane using an Avanti mini extruder (Avestin, Canada).

Characterization of luteolin-loaded PLGA nanoparticles and biomimetic nanoparticles

The particle size and Zeta potential of Lut-NPs and Exo-Lut-NPs were measured by dynamic light scattering (DLS) instrument using Malvern laser particle size analyzer ($n=3$). The Lut-NPs and Exo-Lut-NPs were diluted with deionized water to a final PLGA concentration of 0.1 mg/ml. Subsequently, the nanoparticle samples for TEM imaging were prepared by a routine "negative staining" method as described above. The DLC and EE of luteolin in Lut-NPs and Exo-Lut-NPs were determined with high performance liquid chromatography (HPLC, injection volume, 20 μL; C18 column, 250 mm × 4.6 mm, Kromasil; column temperature, 25 ℃; mobile phase, acetonitrile: 0.2% phosphoric acid 33:77; flow rate, 1 mL/min; and ultraviolet (UV) detection wavelength, 350 nm). The analytical parameters of the HPLC–UV methodology for determining luteolin included the calibration curve, R-squared, linear range, limits of detection (LODs) and limits of quantification (LOQs). Prior to HPLC analysis, Lut-NPs and Exo-Lut-NPs were centrifuged at 12,851 g for 30 min and the nanoparticle pellet was disrupted by acetonitrile to release luteolin. The DLC and EE were calculated using Eqs. (1) and (2), respectively:

$$\text{DLC}\ (\%) = (\text{amount of luteolin loaded}) / (\text{total weight of nanoparticles}) \times 100\% \quad (1)$$

$$\text{EE}\ (\%) = (\text{amount of luteolin loaded}) / (\text{amount of luteolin added}) \times 100\% \quad (2)$$

In vitro release study of Lut-NPs and Exo-Lut-NPs under different pH

In vitro release studies of Lut-NPs and Exo-Lut-NPs were carried out in PBS solution containing 0.5% Tween 80 under physiological (pH 7.4) or acidic (pH 5.5) conditions with the dialysis method. In brief, one milliliter of luteolin, Lut-NPs, and Exo-Lut-NPs suspension with luteolin concentration of 45 μg/mL were added into sealed dialysis bag (MWCO8-14 kDa) separately in 30 mL of drug release media, and kept at 37 ℃ with constant stirring (100 rpm). The one milliliter of the release media was taken at predetermined intervals (0.5, 1 2, 4, 6, 8, 12, 24 and 48 h) and replaced by the fresh release media at the same temperature. The amount of luteolin in the release media was determined with the HPLC–UV method as described before. The luteolin release was quantified using the following equation:

$$\text{Drug release}\ (\%) = (\text{luteolin amount in release media} / \text{luteolin amount in the formulation}) \times 100\% \quad (3)$$

In vitro cellular uptake study

DiD (Tetramethylindodicarbocyanine,4-Chlorobenzenesulfonate Salt) (Meilun, China) was utilized as a fluorescent probe in the cellular uptake study. DiD-NP and Exo-DiD-NP were prepared according to the same method with 200 μg DiD added into acetone instead of luteolin. The LX2 cells uptake of DiD-NP and Exo-DiD-NP was studied using inverted fluorescence microscope. In brief, the LX2 cells were seeded at a density of 1.5×10^4 cells/mL in 24-well plates and cultured for 16 h. After stimulation of TGF-β (10 ng/mL) for 24 h, the cell supernatant was replaced by DiD-NP and Exo-DiD-NP diluted with the culture medium containing the same concentration of DiD (700 ng/well), and incubated for 2 h. After that, 4 ℃ PBS solution was added to terminate the cell uptake and was used to wash the cells three times. Cells were then fixed by 400 μL of 4% paraformaldehyde for 10 min. The cell nucleus was stained by DAPI (MedChemExpress, USA) for 8 min and cells were observed under inverted fluorescence microscope (Leica, Germany). ImageJ was used to quantify the intensity of internalized DiD-labeled nanoparticles in terms of DiD fluorescence intensity normalized to DAPI.

In vitro antitumor effects of biomimetic nanoparticles on the HepG2/LX2 sorafenib-resistant model

In vitro cytotoxicity assay

The cytotoxicity of sorafenib to HepG2 and LX2 cells and the cytotoxicity of luteolin to LX2 cells were evaluated by the 3-(4,5-dimethyl-2-thiazolyl)-2,5-diphenyl-2-H-tetrazolium bromide (MTT) assay (Ruan et al. 2018) to determine the appropriate drug concentrations which were applied to the in vitro HepG2/LX2 sorafenib-resistant

model. Briefly, the HepG2 and LX2 cells were cultured in 96-well plates at a density of 1×10^4 cells/well and incubated at 37 ℃ for 16 h. Sorafenib and luteolin were dissolved in DMSO solution at a concentration of 80 mM, which were diluted by the culture medium to the corresponding concentration (the final DMSO concentration is less than 0.5%). The HepG2 cells were incubated with various concentrations of sorafenib (0.625, 1.25, 2.5, 5, 10, 20, 25, 40, 50, 100 μM) for 48 h. LX2 cells were incubated with various concentrations of luteolin (1.25, 2.5, 5, 10, 20, 40, 50, 100, 150, 200 μM) and sorafenib (0.625, 1.25, 2.5, 5, 10, 20, 40, 50, 100, 150 μM) for 24 h, respectively. After the removal of the culture medium, MTT solution was added to each well and incubated at 37℃ for another 4 h. Finally, the supernatants were replaced with 150 μL of DMSO and shaken for 10 min to dissolve formazan crystals. The absorbance value was measured at 490 nm with the microplate reader (Molecular Device, USA). Dose–response curves were created and used to calculate the 50% inhibitory concentration (IC50) and 80% inhibitory concentration (IC80).

Establishment of the HepG2/LX2 sorafenib-resistant model in vitro

The HepG2 cells are frequently used to establish the sorafenib-resistant HCC model (Sieghart et al. 2012; Prieto-Domínguez et al. 2016). LX2 cells are frequently used to investigate the effect of the interaction between hepatoma cells and hepatic stellate cells on sorafenib resistance in HCC (Rangwala et al. 2012; Khawar et al. 2018). Thus, these two cell lines were selected to establish a HepG2 cell sorafenib-resistant model induced by LX2 cell conditioned medium. Similar to other in vitro drug-resistant models in previous studies, the current HepG2/LX2 sorafenib-resistant model in vitro was established to simulate sorafenib resistance of HepG2 cells induced by HepG2-LX2 cell crosstalk and was used to evaluate the effects of Exo-Lut-NPs on reversing this drug resistance by regulating LX2 cells (Onzi et al. 2016; Liu et al. 2022).

Initially, LX2 cells were seeded into 6-well plates and grown overnight. Then the culture medium was replaced with fresh medium (2 mL/well) supplemented with 10 ng/mL TGF-β for 9 h to induce LX2 cells to an activated state. During this process, after 6-h TGF-β incubation, the media was not removed and sorafenib at different concentrations (8, 20 and 25 μM) was added to incubate the cells for 3 h (the same amount of PBS was added as a control). The medium was then discarded and cells were washed with PBS for 3 times. Finally, the fresh culture medium was added and re-cultivated cells for 48 h to collect the LX2 cell conditioned medium. The different conditioned mediums (CM) after LX2 cells treated with PBS (PBS-CM, as a control group) or sorafenib (8 μM Sorafenib-CM, 20 μM Sorafenib-CM and 25 μM Sorafenib-CM, as model groups) was collected, and centrifuged at 113 g for 5 min, followed by filtration through a 0.45-μm syringe filter (Millipore, USA).

At the same time, the HepG2 cells cultured in 96-well plates at a density of 0.8×10^4 cells/well were incubated at 37 ℃ for 24 h and reached to 70–80% confluence. The medium was then replaced with different CM collected as described above and to assess the effects of different CM on HepG2 resistance to sorafenib (19.5 μM of sorafenib for 48 h) by MTT assays.

Effects of Exo-Lut-NPs on reversing sorafenib resistance on the HepG2/LX2 sorafenib-resistant model in vitro

Based on the sorafenib-resistant model establishment protocol, 9 h of incubation with TGF-β was conducted to stimulate LX2 cells. During this process, after 2 h of TGF-β incubation, i) HepG2 exosomes, ii) PLGA-NPs without loading luteolin, iii) free luteolin, iv) Lut-NPs, and v) Exo-Lut-NPs were added for 4 h, respectively (as shown in Fig. 5A, an equivalent dose of 20 μM luteolin was given in free luteolin, Lut-NPs and Exo-Lut-NPs groups). Then LX2 cells in every group were then incubated with 20 μM of Sorafenib for 3 h except for the control group. The CM of LX2 cells treated with PBS (PBS-CM), sorafenib (20 μM Sorafenib-CM), HepG2 exosomes (Exo-CM), PLGA-NPs without loading luteolin (PLGA-NPs-CM), free luteolin (Free luteolin-CM), Lut-NPs (Lut-NPs-CM) and Exo-Lut-NPs (Exo-Lut-NPs-CM), was collected to replace the culture medium of HepG2 cells. Finally, MTT assays were conducted to determine the effects of sorafenib on HepG2 cell viability with different CM of LX2.

Hemolysis assay of Exo-Lut-NPs

The hemolysis assay was conducted as reported previously (Li et al. 2023). The red blood cells (RBCs) were collected from the whole blood of mice and washed three times with saline (500 g for 10 min). Then the precipitated red blood cells were diluted with saline to obtain 2% RBCs suspension for further use.

The Exo-Lut-NPs with different concentrations of luteolin (1.5, 3, 6, 12 and 24 μg/mL) were mixed with above RBCs suspension and incubated at 37 °C for 1 h to observe the hemolysis. Pure water was used as a positive control and the saline as a negative control. After centrifugation at 2000 g for 5 min, the absorbance of the supernatant at 545 nm was determined using the microplate reader (Thermo, USA). The hemolysis percentage was calculated by Eq. (4). A hemolysis percentage exceeding 5% is considered as hemolysis:

$$\begin{aligned}&\text{Hemolysis percentage (\%)}\\&= \left(\text{sample absorbance} - \text{negative control absorbance}\right)/\\&\left(\text{positive control absorbance} - \text{negative control absorbance}\right)\\&\times 100\%\end{aligned} \tag{4}$$

In vivo antitumor effects of biomimetic nanoparticles combined with sorafenib

The in vivo antitumor efficacy was investigated on a HepG2/LX2 subcutaneous xenograft tumor model to mimic hepatoma cells–HSCs interactions. The tumor-bearing mouse model was established as described previously with some modification. The mixed cell suspension in PBS comprising HepG2 cells (1×10^7 cells) and LX2 cells (1×10^7 cells) was injected into the right armpit of Balb/c nude mice at a total volume of 200 μL (Zhao et al. 2020; Liu et al. 2019b). On the 15th day after tumor inoculation, the tumor volume grew to about 100 mm^3 and these mice were randomly divided into the following four groups ($n = 5$), which were administrated with (i) normal saline (control group); (ii) sorafenib; (iii) sorafenib combined with Lut-NPs; and (iv) sorafenib combined with Exo-Lut-NPs for a 12-day treatment. The Lut-NPs and Exo-Lut-NPs with equivalent luteolin

dose of 0.48 mg/kg were given intravenously every other day (i.v.e.o.d) and sorafenib (50 mg/kg) was given orally every day (p.o.q.d). The tumor volume and body weight of mice were measured every day. The tumor volume was calculated as shown in the following equation:

$$\text{Tumor volume} = \left(\text{Tumor length} \times \text{Tumor width}^2\right) \Big/ 2 \tag{5}$$

Statistical analysis

Statistical analysis was conducted using GraphPad Prism software (Version 8.0.1). T-test analysis was performed to determine differences between the two independent groups, and the differences among three or more groups were analyzed by one-way ANOVA. $P < 0.05$ was considered statistically significant. All data were expressed as mean ± SD. The data were obtained from at least three independent measurements.

Results

Characterization of isolated HepG2 exosomes

To verify that the vesicular bodies extracted from the supernatant of HepG2 cells by differential centrifugation were exosomes, they were characterized for size, size distribution, Zeta potential, particle morphology and exosome-associated proteins. The size distribution measured by qNano (Izon, New Zealand) based on tunable resistive pulse sensing (TRPS) technology presented that the particle size of HepG2 exosomes was

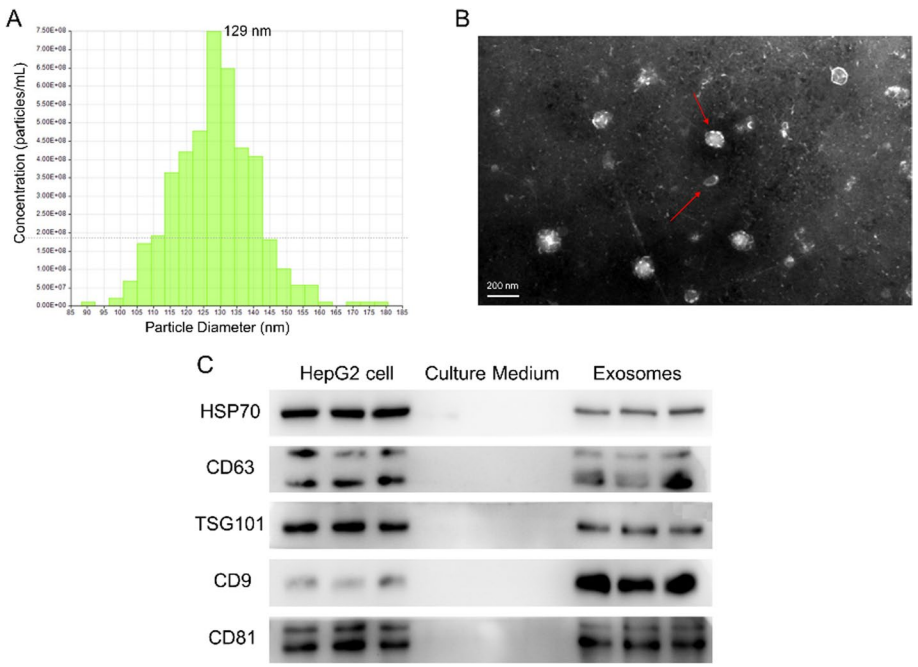

Fig. 1 Characterization of isolated HepG2 exosomes. **A** Particle size distribution with a peak around 129 nm of HepG2 exosomes was detected by qNano. **B** Image of HepG2 exosomes acquired by transmission electron microscopy (TEM). The red arrows indicated the cup-like or saucer-like shape of HepG2 exosomes. **C** Western blotting analysis of exosome markers including heat shock protein 70 (HSP 70), CD63, TSG101, CD9, and CD81 (Positive control: HepG2 cell lysate; Negative control: culture medium)

Table 1 Effects of different luteolin/PLGA ratios on particle size, Zeta potential, DLC and EE of Lut-NPs (n = 3, mean ± SD)

NO	Luteolin/PLGA (w/w)		Particle size (nm)	Zeta potential (mV)	DLC(%)	EE (%)	Luteolin concentration (mg/mL)
	(%)	(mg/mg)					
P1	5	0.526/10	112 ± 4	− 39 ± 1	1.4 ± 0.1	28.6 ± 1.9	0.15 ± 0.01
P2	4	0.420/10	115 ± 5	− 37 ± 1	2.3 ± 0.2	57.1 ± 3.6	0.24 ± 0.02
P3	3	0.310/10	115 ± 3	− 33 ± 3	2.0 ± 0.0	64.7 ± 1.0	0.20 ± 0.00
P4	4	0.210/5	93 ± 7	− 33 ± 2	2.5 ± 0.1	53.6 ± 2.9	0.11 ± 0.01
P5	4	0.840/20	Precipitation				

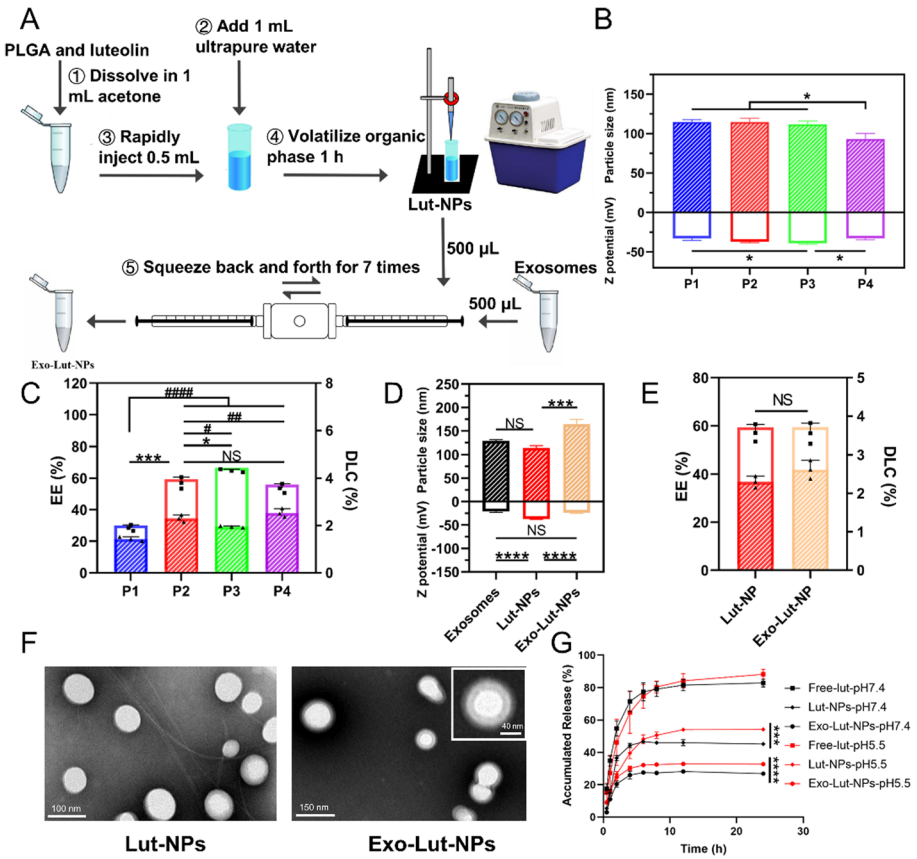

Fig. 2 Preparation and characterization of Lut-NPs and Exo-Lut-NPs. **A** Schematic illustration of the fabrication of Exo-Lut-NPs by the sequential nanoprecipitation and the extrusion method. **B** Particle sizes and Zeta potentials of four kinds of Lut-NPs (P1, P2, P3, P4) with different PLGA solution concentrations and PLGA/luteolin ratios, n = 3, mean ± SD, $^{*}P < 0.5$. **C** Drug loading capacity (DLC) and encapsulation efficiency (EE) of Lut-NPs (P1, P2, P3, P4), $n = 3$, mean ± SD, NS: Not Significant for DLC, $^{*}P < 0.5$ for DLC, $^{***}P < 0.001$ for DLC, $^{\#}P < 0.5$ for EE, $^{\#\#}P < 0.01$ for EE, $^{\#\#\#\#}P < 0.0001$ for EE. **D** Particle sizes and Zeta potentials of HepG2 exosomes, Lut-NPs and Exo-Lut-NPs, $n = 3$, mean ± SD, NS: Not Significant, $^{***}P < 0.001$, $^{****}P < 0.0001$. **E** DLC and EE of Lut-NPs and Exo-Lut-NPs, $n = 3$, mean ± SD, NS: Not Significant for DLC and EE. **F** Representative TEM images of Lut-NPs and Exo-Lut-NPs. **G** In vitro release of luteolin from Lut-NPs and Exo-Lut-NPs in pH 7.4 and pH 5.5 environment, $^{***}P < 0.001$, $^{****}P < 0.0001$

found to be 129 ± 12.3 nm with Zeta potential of -22 ± 2 mV and the particle concentration was 4.41×10^9 particles/mL (Fig. 1A).

The vesicular bodies were further characterized by TEM to study the morphological characteristic. The TEM image displayed the presence of bilayer-membrane vesicles with a typical cup-like or saucer-like shape as described in previous studies (Fig. 1B) (Xu et al. 2021; Wang et al. 2021a). Furthermore, as shown in Fig. 1C, characteristic proteins such as HSP 70, CD63, TSG101, CD9, and CD81 were detected in the HepG2 cell lysate and the isolated exosomes, which confirmed that the vesicular bodies obtained from the cell supernatant were HepG2 exosomes. Overall, the results of qNano, TEM and western blotting analysis demonstrated the successful isolation of HepG2 exosomes.

Characterization of luteolin-loaded PLGA nanoparticles and biomimetic nanoparticles

In consideration of the role of polymer/drug ratios in particle size, Zeta potential, DLC and EE, we compared five kinds of nanoparticles (P1, P2, P3, P4 and P5; see description and composition in Table 1), which were fabricated by nanoprecipitation method with different PLGA solution concentration (5 mg/mL, 10 mg/mL and 20 mg/mL) and PLGA/luteolin ratios (w/w: 5%, 4% and 3%) (Fig. 2A). The DLS measurements revealed that the particle sizes of Lut-NPs (from P1 to P4) were 112 ± 4, 115 ± 5, 115 ± 3 and 93 ± 7 nm, respectively, and Zeta potentials were − 39 ± 1, − 37 ± 1, − 33 ± 3 and − 33 ± 2 mV, respectively (Fig. 2B). The luteolin/PLGA ratio was optimized through P1, P2, P3 in Table 1. The results showed that, 4% luteolin/PLGA resulted in the highest luteolin content in the formulation (0.24 ± 0.02 mg/mL). Since luteolin is an insoluble substance, excessive dosage of luteolin can lead to direct precipitation of the formulation. After comparing the three Luteolin/PLGA (w/w) concentrations at 4% (luteolin/PLGA (w/w)) through P2 (0.420/10), P4 (0.210/5), P5 (0.840/20) (lead to drug precipitation), we chose P2 as the final formulation.

For HPLC–UV analysis of luteolin, LODs and LOQs were 0.03 and 0.1 μg/ml, respectively, and the calibration curve showed good linearity over the range 1–250 μg/mL ($r > 0.9999$). The formulation screening result showed that the content of luteolin in the P2 group was significantly higher than that in the other groups (Fig. 2C), and thus, the P2 formulation (PLGA/luteolin ratio: 4%, 0.420 mg/10 mg) with the highest drug loading was selected to be further coated with exosomes. The particle size of the P2 group was 115 ± 5 nm with a low polydispersity index (PDI) of 0.095 ± 0.027.

The Exo-Lut-NPs were obtained after the mixture and extrusion of the exosomes with Lut-NPs at the polymer/membrane protein ratio of 2:1. The hydrodynamic diameter of the Exo-Lut-NPs was 165 ± 10 nm (PDI: 0.223 ± 0.009) and increased by about 50 nm compared to that of Lut-NPs, and the Zeta potential was − 24 ± 1 mV, which was closer to the exosomal transmembrane potential (Fig. 2D). The DLC and EE of Lut-NPs and Exo-Lut-NPs are shown in Fig. 2E. The TEM images revealed that both Lut-NPs and Exo-Lut-NPs were spherical in shape, with rounded edges and uniform size distribution (Fig. 2F). In addition, Exo-Lut-NPs presented an obvious core–shell structure similar to previous studies, which could not be observed in the TEM images of Lut-NPs (Liu et al. 2019a; Han et al. 2020). Moreover, the size of the nanoparticles estimated from TEM images agreed with the one measured by the Malvern laser particle size analyzer. To sum

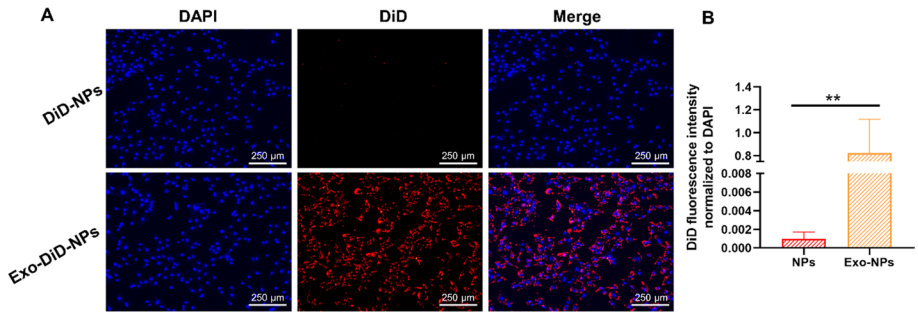

Fig. 3 LX2 cells uptake of DiD-NPs and Exo-DiD-NPs after incubation for 2 h. **A** Inverted fluorescence microscope images of LX2 cells treated with the DiD-NPs and Exo-DiD-NPs, respectively. **B** Intensity of internalized DiD labeled nanoparticles in terms of DiD fluorescence intensity normalized to DAPI quantified by ImageJ ($n = 4$), $^{**}P < 0.01$

up, the increased particle size, Zeta potential and TEM indicated the successful coating of exosomes on the Exo-Lut-NPs surface.

In vitro release study of Lut-NPs and Exo-Lut-NPs under different pH

The in vitro drug release profiles of Lut-NPs and Exo-Lut-NPs at pH 7.4 and pH 5.5 were shown in Fig. 2G. The Lut-NPs and Exo-Lut-NPs showed a significant sustained release compared to free luteolin, and this slow release could be due to the slow degradation of the PLGA. For free luteolin and Lut-NPs, the drug released more rapidly at pH 7.4 than at pH 5.5 within 4 h, whereas the release speed at pH 5.5 caught up with and surpass that at pH 7.4 after 8 h. However, the release of Exo-Lut-NPs at pH 7.4 was consistently slower than that at pH 5.5 which may be caused by the encapsulating of the HepG2 exosomes.

In vitro cellular uptake study

To evaluate the targeting effect of nanoparticles on LX2 cells, we synthesized DiD-NPs and Exo-DiD-NPs. The DiD fluorescence intensity of DiD-NPs and Exo-DiD-NPs in the LX2 cells after 2 h incubation was investigated by inverted fluorescence microscope. As shown in Fig. 3A, the Exo-DiD-NPs showed a significantly higher uptake by LX2 cells, while the DiD-NPs were rarely internalized. Figure 3B demonstrated that the uptake number of Exo-DiD-NPs in the LX2 cells was about 500 times higher than that of DiD-NPs after 2-h incubation, which suggested that coating nanoparticles with HepG2 exosomes significantly enhanced the accumulation of Exo-DiD-NPs in LX2 cells and showed a remarkable LX2 targeting property.

Biomimetic nanoparticles sensitizing hepatoma cells to sorafenib by regulating HSCs in vitro

The MTT results showed that the IC50 of luteolin in LX2 cells (incubation time of 24 h) was 27.3 ± 0.3 μM, and the IC50 of sorafenib in both LX2 cells (incubation time of 24 h) and HepG2 cells (incubation time of 48 h) was 18.49 ± 0.5 and 19.5 ± 0.7 μM (Fig. 4). The IC50 (19.5 ± 0.7 μM) was chosen as the therapeutic concentration of sorafenib against HepG2 cells.

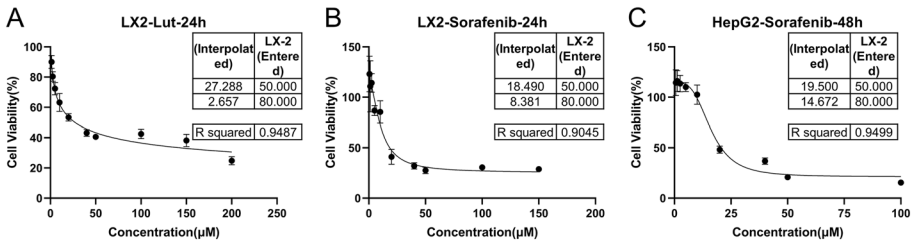

Fig. 4 In vitro cytotoxicity of luteolin and sorafenib at different concentrations to HepG2 cells and LX2 cells. **A** Cell viability of LX2 cells treated with luteolin with increasing dosage for 24 h. **B** Cell viability of LX2 cells treated with sorafenib for 24 h. **C** Cell viability of HepG2 cells treated with sorafenib for 48 h measured by the 3-(4,5-dimethyl-2-thiazolyl)-2,5-diphenyl-2-H-tetrazolium bromide (MTT) assay. IC50 and IC80 were determined by dose–response curves using GraphPad Prism software (Version 8.0.1). Data are represented as mean ± SD ($n = 5$)

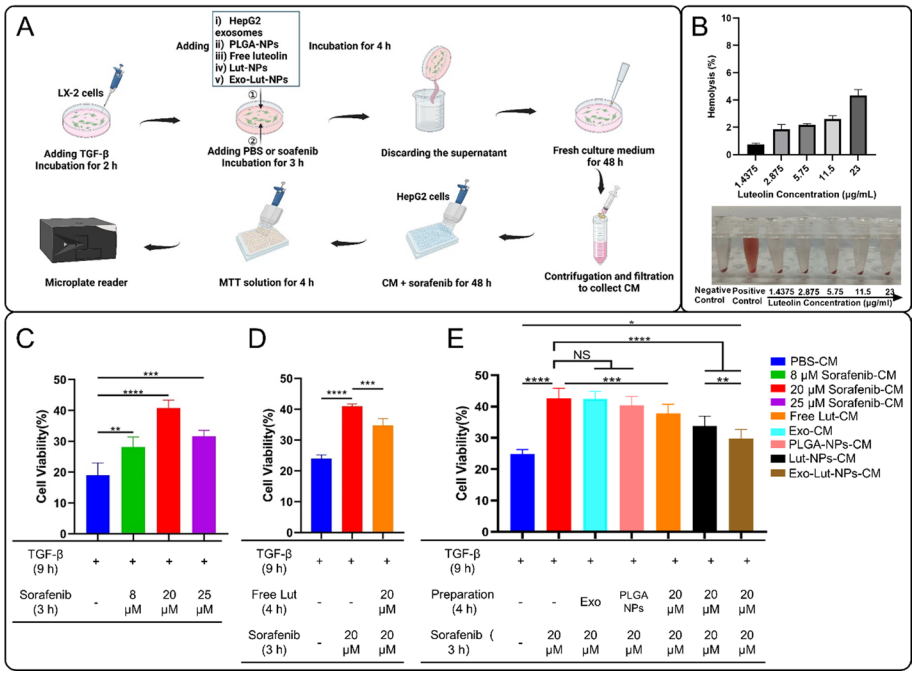

Fig. 5 Exo-Lut-NPs sensitizing hepatoma cells to sorafenib by regulating HSCs on the HepG2/LX2 sorafenib-resistant model in vitro. **A** Schematic illustration of the establishment of the HepG2/LX2 sorafenib-resistant model in vitro. Created with https://www.biorender.com/. Based on the model, the effects of the Exo-Lut-NPs on reversing sorafenib resistance to HepG2 cells via LX2 cells were investigated. **B** Hemolytic test of different concentrations of Exo-Lut-NPs. The hemolysis percentages were assessed 1 h after adding different concentrations of Exo-Lut-NPs. Erythrocytes treated with PBS (0% hemolysis) and distilled water (100% hemolysis) were used as controls. No obvious hemolysis was observed up to 1 mg/ml of Exo-Lut-NPs ($n = 3$, mean ± SD). **C** Culture medium (CM) of LX2 after treated with PBS or sorafenib at different concentrations was collected, including a control group (PBS-CM) and other model groups (8 μM Sorafenib-CM, 20 μM Sorafenib-CM and 25 μM Sorafenib-CM). The effects of different CM on HepG2 resistance to sorafenib were investigated by measuring the cell viability of HepG2 cells after exposure to 19.5 μM sorafenib, aiming to determine the optimum resistance-induced concentration of sorafenib on LX2 cells ($n = 5$, mean ± SD). **D** Effects of the CM of LX2 after treated with free luteolin (20 μM) (Free Lut-CM) on sorafenib resistance of HepG2 were investigated based on the in vitro HepG2/LX2 sorafenib-resistant model (n = 5, mean ± SD). **E** Effects of CM of LX2 cells treated with (i) HepG2 exosomes (Exo-CM), (ii) PLGA-NPs without loading luteolin (PLGA-NPs-CM), (iii) free luteolin (20 μM Free Lut-CM), (iv) Lut-NPs (Lut-NPs-CM), and v) Exo-Lut-NPs (Exo-Lut-NPs-CM) on HepG2 resistance to sorafenib were investigated, respectively. The PBS-CM group was a control group and 20 μM Sorafenib-CM was a model group ($n = 3$, mean ± SD). NS: Not Significant, $^{**}P < 0.01$, $^{***}P < 0.001$, $^{****}P < 0.0001$

The current LX2-conditioned media model can simply avoid unknown stimulation of HepG2 cells by TGF-β and unknown inevitable interference of the hepatocellular carcinoma cells on LX2 cells. So the conditional medium model, which is widely used to study the interaction between cancer cells and their stromal microenvironment (Onzi et al. 2016; Liu et al. 2022), was adopt in our study to explore alleviation effects of the hepatic stellate cells on sorafenib resistant of hepatocellular carcinoma cells. The effect of crosstalk between hepatoma cells and HSCs on the drug resistance of hepatoma cells was evaluated by determining the sorafenib resistance of HepG2 cells which were cultivated in the CM of activated LX2 cells (Fig. 5A). In this process, activated LX2 with or without treatment secreted various cytokines, which contributed to the crosstalk between HepG2 and LX2 (Ligorio et al. 2019; Lenggenhager et al. 2019). As shown in Fig. 5C, compared with the PBS-CM group, the HepG2 cells cultivated in a sorafenib-CM of LX2 cells were strongly refractory to sorafenib. While HepG2 cells were incubated with 8, 20, and 25 μM sorafenib-CM, the inhibitory effect of sorafenib on HepG2 cell proliferation decreased by 9%, 21% and 11%, respectively, which indicated that the sorafenib resistance of hepatoma cells was produced by cancer-stroma crosstalk. Amongst, the 20 μM sorafenib-CM, which could induce the most significant sorafenib resistance of HepG2 cells, was used in the following study to construct the HepG2/LX2 sorafenib-resistant model in vitro. Figure 5D presented that the resistance was partially reversed when HepG2 cells were incubated with the free luteolin-CM, implying that luteolin could adjust LX2 cells and affect cancer-stroma crosstalk to sensitize HepG2 cells to sorafenib. In addition, Lut-NPs-CM and Exo-Lut-NPs-CM further alleviated the drug resistance of HepG2 cells to sorafenib, among which the Exo-Lut-NPs group showed the greatest alleviation effect (Fig. 5E). However, the exosomes-CM group and the PLGA-NPs-CM group exhibited similar sorafenib resistance of HepG2 cells as the model group (20 μM Sorafenib-CM). This result not only indicated that exosomes and blank PLGA nanoparticles did not alleviate the sorafenib resistance, but also suggested that they could not interact with TGF-β or prevent it from exerting its action on LX2 cells. Overall, these results presented that Exo-Lut-NPs treatment of LX2 affected the CM of HSC and partially reversed the sorafenib resistance of HepG2 cells.

The hemolysis assay results showed that Exo-Lut-NPs were highly biocompatible and would not result in hemolysis (Fig. 5B), demonstrating that Exo-Lut-NPs would be non-toxic toward RBCs after i.v. administration.

In vivo antitumor effects of sorafenib combined with biomimetic nanoparticles

The subcutaneous tumor xenograft model is a classical animal model for cancer research (Bárcena et al. 2015; Pittala et al. 2018; Liu et al. 2006; Lee et al. 2018). Subcutaneous tumors were formed after subaxillary injection of the mixture of HepG2 and LX2 cells into nude mice and evaluated by tumor volume and mouse weight. Visible tumor formation was noted and reached 100 mm^3 on the 15th day after implantation of 1.0×10^7 HepG2 cells and 1.0×10^7 LX2 cells (Fig. 6A). After 12 days, the tumor grew up to 2000 mm^3 without significant weight loss in mice, simulating a tumor-bearing state (Fig. 6B, and C). In comparison with the sorafenib group, the combined administration of sorafenib (oral treatment) and Lut-NPs or Exo-Lut-NPs (intravenous injection) significantly retarded tumor growth within 12 days. More importantly, sorafenib combined

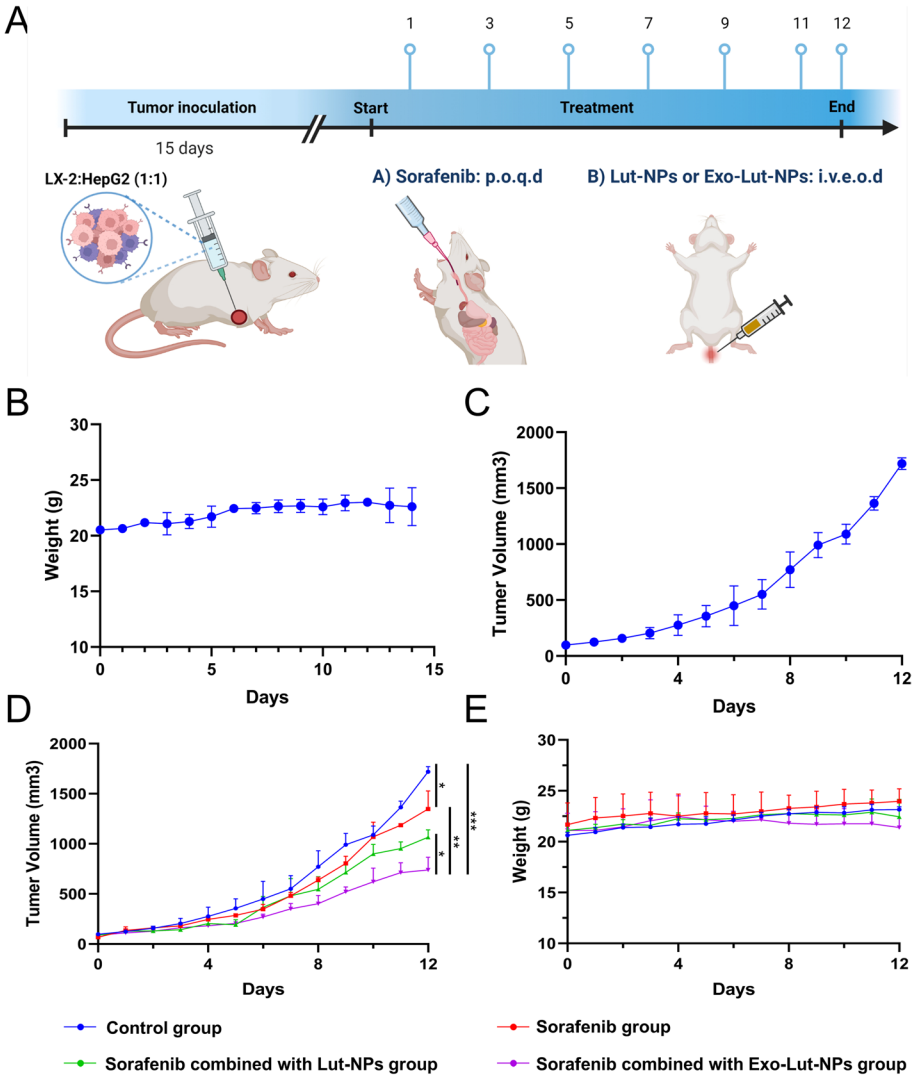

Fig. 6 In vivo combined antitumor effects of Exo-Lut-NPs and sorafenib on a HepG2/LX2 subcutaneous xenograft tumor model. **A** Schematic illustration of the establishment of HCC subcutaneous xenograft mouse model of HepG2 cells and LX2 cells, and the following treatment schedule. Created with https://www.biorender.com/. **B** Body weight of tumor-bearing mice before treatment. **C** Tumor growth trend of the tumor-bearing mice in the control group. **D** Tumor growth trend after different treatments, which were (i) normal saline (control group), (ii) sorafenib (50 mg/kg), (iii) sorafenib (50 mg/kg) combined with Lut-NPs (equivalent luteolin dose of 0.48 mg/kg), and (iv) sorafenib (50 mg/kg) combined with Exo-Lut-NPs (equivalent luteolin dose of 0.48 mg/kg) for a 12-day treatment. **E** Body weight of tumor-bearing mice after different treatment. Data are represented as mean ± SD ($n = 5$), *$P < 0.05$, **$P < 0.01$, ***$P < 0.001$

with the Exo-Lut-NPs group exhibited the best effect on retardation of tumor growth ($P < 0.001$) (Fig. 6C, and D). As a result, the combination treatment of sorafenib and Exo-Lut-NPs enhanced the inhibition effect of sorafenib on tumor progression. Furthermore, no abnormal weight loss had been observed following different treatments, which reflected the acceptable safety of the treatments applied in this study.

Discussion

The interaction between HSCs and hepatoma cells in the tumor microenvironment promotes the drug resistance of HCC patients to sorafenib, which remains a great challenge of HCC treatment. Luteolin is regarded as a promising HCC therapy that can dampen the proliferation of activated HSCs, but exerts modest effects owing to its low water solubility and bioavailability. What's more, as sorafenib combined with luteolin killed HCC cells through JNK-mediated apoptosis (Feng et al. 2018), luteolin may be an ideal candidate for increasing the activity of sorafenib in HCC therapy. To evaluate the antitumor effects of Exo-Lut-NPs combined with sorafenib, we established a sorafenib-resistant HepG2 cell model via remodeling LX2 cells in vitro and an HCC subcutaneous xenograft mouse model in vivo. The aforesaid results demonstrated that luteolin-loaded biomimetic nanoparticles exhibited good potential with sorafenib for HCC treatment.

The CD9 is a transmembrane protein and is considered as a bio-marker of cell membranes and extracellular vesicles. Thus, exosomes, which are released into the extracellular matrix after fusion with the cell membrane through their outer membrane, carry more cell transmembrane proteins like CD9. A previous study showed that the CD9 expression on the extracellular vesicles is higher than that expression on the Hela cell lysates (Mathieu et al. 2021), so as LAMP expression on HepG2^{Cyp2E1} cells (Verma et al. 2016). In our study, the results also showed that the CD9 expression on the HepG2 exosomes is much higher than that on the HepG2 cell lysates which is correlated with previous studies.

In our study, luteolin-loaded PLGA nanoparticles greatly enhanced the solubility and bioavailability of luteolin. The water solubility of luteolin is 0.0064 mg/mL (Chen et al. 2022) which greatly limited its usage and the Exo-Lut-NPs can be administrated at a concentration of 0.240 ± 0.015 mg/mL (37.5 times that of free luteolin). Considering the operation difficulty and the influence on the integrity of the exosomes, the extrusion method is the most suitable method for the coating nanoparticles with exosome membranes (Agrawal et al. 2017; Kim et al. 2016; Faruqu et al. 2018; Haney et al. 2015; Shany et al. 1974; Wang et al. 2021b). Exosome-coated PLGA nanoparticles we fabricated displayed a more uniform size distribution and higher incorporation efficiency compared with exosomes loading drugs directly (Liu et al. 2019a; Ashour et al. 2022). In addition, the similarity of Zeta potential between pure exosomes and Exo-Lut-NPs also confirmed the successful coating of exosome membranes.

In the tumor microenvironment, HCC cells exhibited a great capacity to transmit exosomes to HSCs which may lead to HSC activation and liver fibrosis (Zhou et al. 2018; Xie et al. 2022). Exosomes released by different liver cancer cells have been proven to be delivered to HSCs (Zhou et al. 2018; Feng et al. 2022), among which HepG2 exosomes intuitively demonstrated their HSC targeting ability through a cellular uptake experiment (Feng et al. 2022). This study also confirmed that HepG2 exosomes coated nanoparticles could also target hepatic stellate cells and significantly increase their uptake of nanoparticles. The controlled release properties and better targeting efficiency of Exo-Lut-NPs to HSC will also help luteolin to induce therapeutic benefits at a relative lower dose.

To evaluate whether luteolin-loaded biomimetic nanoparticles can be combined with sorafenib to enhance therapeutic effects by regulating hepatic stellate cells, we constructed the CM model of LX2 cells. The Hyo-Jeong Kuh team developed a mixed cell

sphere model using Huh-7 HCC cells and LX2 cells to simulate the interaction of tumor CAF in the tumor environment in vitro (Khawar et al. 2018). The results showed that the presence of LX2 cells would reduce the efficacy of sorafenib in the mixed cell sphere. In our study, we confirmed for the first time that the CM of LX2 cells can induce resistance of HepG2 to sorafenib. The TGF-β-activated HSCs induced drug resistance of HepG2 cells to sorafenib in vitro, which could be partially alleviated by the effect of free luteolin, Lut-NPs and Exo-Lut-NPs on the CM of HSCs. Similarly, the Exo-Lut-NPs group combined with sorafenib exhibited an excellent combined effect on retardation of tumor growth in the subcutaneous xenograft tumor mice model compared to the sorafenib alone and Lut-NPs group combined with sorafenib in vivo.

It was found in clinical samples that CD36 + cancer-associated fibroblasts (CAFs) derived from hepatic stellate cells led to the immunotherapy-resistant microenvironment for hepatocellular carcinoma (Zhu et al. 2023). After co-culturing with HCC cells, HSC secreted more hepatocyte growth factor to stimulate the expression of the oncogene STMN1 in HCC cells concomitant with vascular invasion, higher histological grade, advanced clinical grade, shorter survival time and worse drug resistance (Zhang et al. 2020). Therefore, hepatic stellate cells play an important role in the development and progression of drug resistance in liver cancer. In this study, we adopt targeted regulation to regulate HSC. Based on the in vivo and in vitro models, the regulation effects of Exo-Lut-NPs on drug resistance and the impact on tumor growth were verified and showed promising clinical relevance. Further studies will be carried out to confirm the apoptosis of the tumors and elucidate the mechanism by which the luteolin HSCs targeting strategy improved sorafenib therapy on HCC.

Conclusion

In this study, we constructed a novel biomimetic nano-delivery system Exo-Lut-NPs, which is composed of HepG2 exosomes coated luteolin nanoparticles. This nano-delivery system effectively alleviated sorafenib resistance in vitro as well as demonstrated improved anti-hepatocellular carcinoma effects in vivo when combined application with sorafenib, which provides a novel therapeutic schedule for alleviating clinical sorafenib resistance and enhancing the treatment effect of sorafenib on hepatocellular carcinoma. The mechanism by which the luteolin HSCs targeting strategy improved sorafenib therapy on HCC as well as the biodistribution and safety of Exo-Lut-NPs will be further validated.

Supplementary Information

The online version contains supplementary material available at https://doi.org/10.1186/s12645-024-00253-7.

Additional file 1. The short tandem repeats (STR)identification results of HepG2 cells and LX2 cells.

Acknowledgements

The authors gratefully acknowledge the Department of Hepatology, Shuguang Hospital, Shanghai University of Traditional Chinese Medicine for assistance with cell supply. Figures 2A, 4A and 5A show generated using https://www.biorender.com/.

Funding

This research was funded by the National Natural Science Foundation of China (Grant No. 81773909), Shanghai Talent Development Funds (Grant No.201665, China), Shanghai Municipal Commission of Health and Family Planning (Grant No. 2017YQ060, China), "Shuguang Program" supported by Shanghai Education Development Foundation and Shanghai Municipal Education Commission (Grant No. 22SG41), the combination of the medical care and health project of the Shanghai University of Traditional Chinese Medicine (YYKC-2021-01-008), and Construction Project of Shanghai Innovation Center of TCM Health Service (A1-U23-308-01).

Availability of data and materials
The data sets used and/or analyzed during the current study are available from the corresponding author on reasonable request.

Declarations

Author contributions
Conceptualization: SY, KH, YH and LZh. Methodology: SY and KH. Software: SY and XP. Validation: SY and XP. Formal analysis: SY, XP and KH. Investigation: SY and KH. Resources: SY and KH. Data curation: SY and XP. Writing—original draft preparation: SY. Writing—review and editing: SY, XP, SN, LZo and KH. Visualization: SY and XP. Supervision; KH, YH and LZh. Project administration: KH. funding acquisition: KH, YH and LZh. All authors have read and agreed to the published version of the manuscript.

Ethics approval and consent to participate
All institutional and national guidelines for the care and use of laboratory animals were followed.

Consent for publication
Not applicable.

Competing interests
The authors declare that they have no competing interests.

Received: 24 September 2023 Accepted: 29 January 2024
Published online: 22 February 2024

References

Abou-Alfa GK, Johnson P, Knox JJ, Capanu M, Davidenko I, Lacava J, Leung T, Gansukh B, Saltz LB (2010) Doxorubicin plus sorafenib vs doxorubicin alone in patients with advanced hepatocellular carcinoma: a randomized trial. JAMA 304:2154–2160. https://doi.org/10.1001/jama.2010.1672

Agrawal AK, Aqil F, Jeyabalan J, Spencer WA, Beck J, Gachuki BW, Alhakeem SS, Oben K, Munagala R, Bondada S, Gupta RC (2017) Milk-derived exosomes for oral delivery of paclitaxel. Nanomedicine 13:1627–1636. https://doi.org/10.1016/j.nano.2017.03.001

Ashour AA, El-Kamel AH, Mehanna RA, Mourad G, Heikal LA (2022) Luteolin-loaded exosomes derived from bone marrow mesenchymal stem cells: a promising therapy for liver fibrosis. Drug Deliv 29:3270–3280. https://doi.org/10.1080/10717544.2022.2142700

Azzariti A, Mancarella S, Porcelli L, Quatrale AE, Caligiuri A, Lupo L, Dituri F, Giannelli G (2016) Hepatic stellate cells induce hepatocellular carcinoma cell resistance to sorafenib through the laminin-332/α3 integrin axis recovery of focal adhesion kinase ubiquitination. Hepatology 64:2103–2117. https://doi.org/10.1002/hep.28835

Bárcena C, Stefanovic M, Tutusaus A, Martinez-Nieto GA, Martinez L, García-Ruiz C, de Mingo A, Caballeria J, Fernandez-Checa JC, Marí M, Morales A (2015) Angiogenin secretion from hepatoma cells activates hepatic stellate cells to amplify a self-sustained cycle promoting liver cancer. Sci Rep 5:7916. https://doi.org/10.1038/srep07916

Chakrabarti M, Ray SK (2015) Synergistic anti-tumor actions of luteolin and silibinin prevented cell migration and invasion and induced apoptosis in glioblastoma SNB19 cells and glioblastoma stem cells. Brain Res 1629:85–93. https://doi.org/10.1016/j.brainres.2015.10.010

Chang L-W, Hou M-L, Tsai T-H (2014) Silymarin in liposomes and ethosomes: pharmacokinetics and tissue distribution in free-moving rats by high-performance liquid chromatography-tandem mass spectrometry. J Agric Food Chem 62:11657–11665. https://doi.org/10.1021/jf504139g

Chen Q, Chen J, Yang Z, Xu J, Xu L, Liang C, Han X, Liu Z (2019) Nanoparticle-enhanced radiotherapy to trigger robust cancer immunotherapy. Adv Mater 31:e1802228. https://doi.org/10.1002/adma.201802228

Chen L, Chang S, Zhao L, Li B, Zhang S, Yun C, Wu X, Meng J, Li G, Guo S, Duan J (2022) Biosynthesis of a water solubility-enhanced succinyl glucoside derivative of luteolin and its neuroprotective effect. Microb Biotechnol 15:2401–2410. https://doi.org/10.1111/1751-7915.14095

Copp JA, Fang RH, Luk BT, Hu C-MJ, Gao W, Zhang K, Zhang L (2014) Clearance of pathological antibodies using biomimetic nanoparticles. Proc Natl Acad Sci USA 111:13481–13486. https://doi.org/10.1073/pnas.1412420111

Cummins CB, Wang X, Nunez Lopez O, Graham G, Tie H-Y, Zhou J, Radhakrishnan RS (2018) Luteolin-mediated inhibition of hepatic stellate cell activation via suppression of the STAT3 pathway. Int J Mol Sci 19:1567. https://doi.org/10.3390/ijms19061567

D'Ambrosio DN, Walewski JL, Clugston RD, Berk PD, Rippe RA, Blaner WS (2011) Distinct populations of hepatic stellate cells in the mouse liver have different capacities for retinoid and lipid storage. PLoS ONE 6:e24993. https://doi.org/10.1371/journal.pone.0024993

Eisai and merck and CO., INC (2018) kenilworth, N.J., U.S.A. announce FDA approval of lenvima® (lenvatinib) capsules for first-line treatment of unresectable hepatocellular carcinoma (HCC), news release: 2018, Eisai Co., Ltd. https://www.eisai.com/news/2018/news201870.html. Accessed 2 July 2023

European Association For The Study Of The Liver, European Organisation For Research And Treatment Of Cancer (2012) EASL-EORTC clinical practice guidelines: management of hepatocellular carcinoma. J Hepatol 56:908–943. https://doi.org/10.1016/j.jhep.2011.12.001

Fang RH, Hu C-MJ, Luk BT, Gao W, Copp JA, Tai Y, O'Connor DE, Zhang L (2014) Cancer cell membrane-coated nanoparticles for anticancer vaccination and drug delivery. Nano Lett 14:2181–2188. https://doi.org/10.1021/nl500618u

Faruqu FN, Xu L, Al-Jamal KT (2018) Preparation of exosomes for siRNA delivery to cancer cells. J vis Exp. https://doi.org/10.3791/58814
Feng X-Q, Rong L-W, Wang R-X, Zheng X-L, Zhang L, Zhang L, Lin Y, Wang X, Li Z-P (2018) Luteolin and sorafenib combination kills human hepatocellular carcinoma cells through apoptosis potentiation and JNK activation. Oncol Lett 16:648–653. https://doi.org/10.3892/ol.2018.8640
Feng T, Fang F, Zhang C, Li T, He J, Shen Y, Yu H, Liu X (2022) Fluid shear stress-induced exosomes from liver cancer cells promote activation of cancer-associated fibroblasts via IGF2-PI3K axis. Front Biosci (landmark Ed). 27:104. https://doi.org/10.31083/j.fbl2703104
Friedman SL (2008) Hepatic stellate cells: protean, multifunctional, and enigmatic cells of the liver. Physiol Rev 88:125–172. https://doi.org/10.1152/physrev.00013.2007
Grandhi MS, Kim AK, Ronnekleiv-Kelly SM, Kamel IR, Ghasebeh MA, Pawlik TM (2016) Hepatocellular carcinoma: from diagnosis to treatment. Surg Oncol 25:74–85. https://doi.org/10.1016/j.suronc.2016.03.002
Han Z, Lv W, Li Y, Chang J, Zhang W, Liu C, Sun J (2020) Improving tumor targeting of exosomal membrane-coated polymeric nanoparticles by conjugation with aptamers. ACS Appl Bio Mater 3:2666–2673. https://doi.org/10.1021/acsabm.0c00181
Haney MJ, Klyachko NL, Zhao Y, Gupta R, Plotnikova EG, He Z, Patel T, Piroyan A, Sokolsky M, Kabanov AV, Batrakova EV (2015) Exosomes as drug delivery vehicles for Parkinson's disease therapy. J Control Release 207:18–30. https://doi.org/10.1016/j.jconrel.2015.03.033
Higashi T, Friedman SL, Hoshida Y (2017) Hepatic stellate cells as key target in liver fibrosis. Adv Drug Deliv Rev 121:27–42. https://doi.org/10.1016/j.addr.2017.05.007
Hu C-MJ, Zhang L, Aryal S, Cheung C, Fang RH, Zhang L (2011) Erythrocyte membrane-camouflaged polymeric nanoparticles as a biomimetic delivery platform. Proc Natl Acad Sci USA 108:10980–10985. https://doi.org/10.1073/pnas.1106634108
Khawar IA, Park JK, Jung ES, Lee MA, Chang S, Kuh H-J (2018) Three dimensional mixed-cell spheroids mimic stroma-mediated chemoresistance and invasive migration in hepatocellular carcinoma. Neoplasia 20:800–812. https://doi.org/10.1016/j.neo.2018.05.008
Kim MS, Haney MJ, Zhao Y, Mahajan V, Deygen I, Klyachko NL, Inskoe E, Piroyan A, Sokolsky M, Okolie O, Hingtgen SD, Kabanov AV, Batrakova EV (2016) Development of exosome-encapsulated paclitaxel to overcome MDR in cancer cells. Nanomedicine 12:655–664. https://doi.org/10.1016/j.nano.2015.10.012
Kouwaki T, Fukushima Y, Daito T, Sanada T, Yamamoto N, Mifsud EJ, Leong CR, Tsukiyama-Kohara K, Kohara M, Matsumoto M, Seya T, Oshiumi H (2016) Extracellular vesicles including exosomes regulate innate immune responses to hepatitis B virus infection. Front Immunol 7:335. https://doi.org/10.3389/fimmu.2016.00335
Lee Y, Kwon YH (2019) Regulation of apoptosis and autophagy by luteolin in human hepatocellular cancer Hep3B cells. Biochem Biophys Res Commun 517:617–622. https://doi.org/10.1016/j.bbrc.2019.07.073
Lee NP, Chan CM, Tung LN, Wang HK, Law S (2018) Tumor xenograft animal models for esophageal squamous cell carcinoma. J Biomed Sci 25:66. https://doi.org/10.1186/s12929-018-0468-7
Lenggenhager D, Amrutkar M, Sántha P, Aasrum M, Löhr J-M, Gladhaug IP, Verbeke CS (2019) Commonly used pancreatic stellate cell cultures differ phenotypically and in their interactions with pancreatic cancer cells. Cells 8:23. https://doi.org/10.3390/cells8010023
Li T, Shi Z, Rockey DC (2012) Preproendothelin-1 expression is negatively regulated by IFNγ during hepatic stellate cell activation. Am J Physiol Gastrointest Liver Physiol 302:G948-957. https://doi.org/10.1152/ajpgi.00359.2011
Li L, Piontek K, Ishida M, Fausther M, Dranoff JA, Fu R, Mezey E, Gould SJ, Fordjour FK, Meltzer SJ, Sirica AE, Selaru FM (2017) Extracellular vesicles carry microRNA-195 to intrahepatic cholangiocarcinoma and improve survival in a rat model. Hepatology 65:501–514. https://doi.org/10.1002/hep.28735
Li S, Wu Y, Ding F, Yang J, Li J, Gao X, Zhang C, Feng J (2020) Engineering macrophage-derived exosomes for targeted chemotherapy of triple-negative breast cancer. Nanoscale 12:10854–10862. https://doi.org/10.1039/d0nr00523a
Li H, Wang X, Guo X, Wan Q, Teng Y, Liu J (2022) Development of rapamycin-encapsulated exosome-mimetic nanoparticles-in-PLGA microspheres for treatment of hemangiomas. Biomed Pharmacother 148:112737. https://doi.org/10.1016/j.biopha.2022.112737
Li Y, Wu J, Qiu X, Dong S, He J, Liu J, Xu W, Huang S, Hu X, Xiang D-X (2023) Bacterial outer membrane vesicles-based therapeutic platform eradicates triple-negative breast tumor by combinational photodynamic/chemo-/immunotherapy. Bioact Mater 20:548–560. https://doi.org/10.1016/j.bioactmat.2022.05.037
Ligorio M, Sil S, Malagon-Lopez J, Nieman LT, Misale S, Di Pilato M, Ebright RY, Karabacak MN, Kulkarni AS, Liu A, Vincent Jordan N, Franses JW, Philipp J, Kreuzer J, Desai N, Arora KS, Rajurkar M, Horwitz E, Neyaz A, Tai E, Magnus NKC, Vo KD, Yashaswini CN, Marangoni F, Boukhali M, Fatherree JP, Damon LJ, Xega K, Desai R, Choz M, Bersani F, Langenbucher A, Thapar V, Morris R, Wellner UF, Schilling O, Lawrence MS, Liss AS, Rivera MN, Deshpande V, Benes CH, Maheswaran S, Haber DA, Fernandez-Del-Castillo C, Ferrone CR, Haas W, Aryee MJ, Ting DT (2019) Stromal microenvironment shapes the intratumoral architecture of pancreatic cancer. Cell 178:160–175. https://doi.org/10.1016/j.cell.2019.05.012
Lin H, Zhang R, Wu W, Lei L (2021) miR-4454 promotes hepatic carcinoma progression by targeting Vps4A and Rab27A. Oxid Med Cell Longev 2021:9230435. https://doi.org/10.1155/2021/9230435
Liu L, Cao Y, Chen C, Zhang X, McNabola A, Wilkie D, Wilhelm S, Lynch M, Carter C (2006) Sorafenib blocks the RAF/MEK/ERK pathway, inhibits tumor angiogenesis, and induces tumor cell apoptosis in hepatocellular carcinoma model PLC/PRF/5. Cancer Res 66:11851–11858. https://doi.org/10.1158/0008-5472.CAN-06-1377
Liu Y, Yue H, Xu S, Wang F, Ma N, Li K, Qiao L, Wang J (2015) First-line gemcitabine and oxaliplatin (GEMOX) plus sorafenib, followed by sorafenib as maintenance therapy, for patients with advanced hepatocellular carcinoma: a preliminary study. Int J Clin Oncol 20:952–959. https://doi.org/10.1007/s10147-015-0796-5
Liu C, Zhang W, Li Y, Chang J, Tian F, Zhao F, Ma Y, Sun J (2019a) Microfluidic sonication to assemble exosome membrane-coated nanoparticles for immune evasion-mediated targeting. Nano Lett 19:7836–7844. https://doi.org/10.1021/acs.nanolett.9b02841

Liu J, Chang B, Li Q, Xu L, Liu X, Wang G, Wang Z, Wang L (2019b) Redox-responsive dual drug delivery nanosystem suppresses cancer repopulation by abrogating doxorubicin-promoted cancer stemness, metastasis, and drug resistance. Adv Sci (weinh) 6:1801987. https://doi.org/10.1002/advs.201801987
Liu Y, Wu X, Chen F, Li H, Wang T, Liu N, Sun K, Zhou G, Tao K (2022) Modulating cancer-stroma crosstalk by a nanoparticle-based photodynamic method to pave the way for subsequent therapies. Biomaterials 289:121813. https://doi.org/10.1016/j.biomaterials.2022.121813
Luo N, Li J, Chen Y, Xu Y, Wei Y, Lu J, Dong R (2021) Hepatic stellate cell reprogramming via exosome-mediated CRISPR/dCas9-VP64 delivery. Drug Deliv 28:10–18. https://doi.org/10.1080/10717544.2020.1850917
Ma X, Qiu Y, Sun Y, Zhu L, Zhao Y, Li T, Lin Y, Ma D, Qin Z, Sun C, Han L (2020) NOD2 inhibits tumorigenesis and increases chemosensitivity of hepatocellular carcinoma by targeting AMPK pathway. Cell Death Dis 11:174. https://doi.org/10.1038/s41419-020-2368-5
Maheswaran T, Rushbrook SM (2012) Epithelial–mesenchymal transition and the liver: role in hepatocellular carcinoma and liver fibrosis. J Gastroenterol Hepatol 27:418–420. https://doi.org/10.1111/j.1440-1746.2012.07060.x
Marcucci F, Stassi G, De Maria R (2016) Epithelial–mesenchymal transition: a new target in anticancer drug discovery. Nat Rev Drug Discov 15:311–325. https://doi.org/10.1038/nrd.2015.13
Mathieu M, Névo N, Jouve M, Valenzuela JI, Maurin M, Verweij FJ, Palmulli R, Lankar D, Dingli F, Loew D, Rubinstein E (2021) Specificities of exosome versus small ectosome secretion revealed by live intracellular tracking of CD63 and CD9. Nat Commun. https://doi.org/10.1038/s41467-021-24384-2
Niu G, Zhang X, Hong R, Yang X, Gu J, Song T, Hu Z, Chen L, Wang X, Xia J, Ke Z, Ren J, Hong L (2021) GJA1 promotes hepatocellular carcinoma progression by mediating TGF-β-induced activation and the epithelial-mesenchymal transition of hepatic stellate cells. Open Med (wars) 16:1459–1471. https://doi.org/10.1515/med-2021-0344
Onzi GR, Ledur PF, Hainzenreder LD, Bertoni APS, Silva AO, Lenz G, Wink MR (2016) Analysis of the safety of mesenchymal stromal cells secretome for glioblastoma treatment. Cytotherapy 18:828–837. https://doi.org/10.1016/j.jcyt.2016.03.299
Pei W, Li X, Bi R, Zhang X, Zhong M, Yang H, Zhang Y, Lv K (2021) Exosome membrane-modified M2 macrophages targeted nanomedicine: treatment for allergic asthma. J Control Release 338:253–267. https://doi.org/10.1016/j.jconrel.2021.08.024
Pinto M, Silva V, Barreiro S, Silva R, Remião F, Borges F, Fernandes C (2022) Brain drug delivery and neurodegenerative diseases: polymeric PLGA-based nanoparticles as a forefront platform. Ageing Res Rev 79:101658. https://doi.org/10.1016/j.arr.2022.101658
Pittala S, Krelin Y, Shoshan-Barmatz V (2018) Targeting liver cancer and associated pathologies in mice with a mitochondrial VDAC1-based peptide. Neoplasia 20:594–609. https://doi.org/10.1016/j.neo.2018.02.012
Prieto-Domínguez N, Ordóñez R, Fernández A, Méndez-Blanco C, Baulies A, Garcia-Ruiz C, Fernández-Checa JC, Mauriz JL, González-Gallego J (2016) Melatonin-induced increase in sensitivity of human hepatocellular carcinoma cells to sorafenib is associated with reactive oxygen species production and mitophagy. J Pineal Res 61:396–407. https://doi.org/10.1111/jpi.12358
Qiu Z, Li H, Zhang Z, Zhu Z, He S, Wang X, Wang P, Qin J, Zhuang L, Wang W, Xie F, Gu Y, Zou K, Li C, Li C, Wang C, Cen J, Chen X, Shu Y, Zhang Z, Sun L, Min L, Fu Y, Huang X, Lv H, Zhou H, Ji Y, Zhang Z, Meng Z, Shi X, Zhang H, Li Y, Hui L (2019) A pharmacogenomic landscape in human liver cancers. Cancer Cell 36:179-193.e11. https://doi.org/10.1016/j.ccell.2019.07.001
Rangwala F, Williams KP, Smith GR, Thomas Z, Allensworth JL, Lyerly HK, Diehl AM, Morse MA, Devi GR (2012) Differential effects of arsenic trioxide on chemosensitization in human hepatic tumor and stellate cell lines. BMC Cancer 12:402. https://doi.org/10.1186/1471-2407-12-402
Ruan C, Liu L, Lu Y, Zhang Y, He X, Chen X, Zhang Y, Chen Q, Guo Q, Sun T, Jiang C (2018) Substance P-modified human serum albumin nanoparticles loaded with paclitaxel for targeted therapy of glioma. Acta Pharm Sin B 8:85–96. https://doi.org/10.1016/j.apsb.2017.09.008
Ruan Q, Wang H, Burke LJ, Bridle KR, Li X, Zhao C-X, Crawford DHG, Roberts MS, Liang X (2020) Therapeutic modulators of hepatic stellate cells for hepatocellular carcinoma. Int J Cancer 147:1519–1527. https://doi.org/10.1002/ijc.32899
Ruman U, Fakurazi S, Masarudin MJ, Hussein MZ (2020) Nanocarrier-based therapeutics and theranostics drug delivery systems for next generation of liver cancer nanodrug modalities. Int J Nanomedicine 15:1437–1456. https://doi.org/10.2147/IJN.S236927
Seitz T, Freese K, Dietrich P, Thasler WE, Bosserhoff A, Hellerbrand C (2020) Fibroblast growth factor 9 is expressed by activated hepatic stellate cells and promotes progression of hepatocellular carcinoma. Sci Rep 10:4546. https://doi.org/10.1038/s41598-020-61510-4
Shany S, Bernheimer AW, Grushoff PS, Kim KS (1974) Evidence for membrane cholesterol as the common binding site for cereolysin, streptolysin O and saponin. Mol Cell Biochem 3:179–186. https://doi.org/10.1007/BF01686643
Shiraha H, Iwamuro M, Okada H (2020) Hepatic stellate cells in liver tumor. Adv Exp Med Biol 1234:43–56. https://doi.org/10.1007/978-3-030-37184-5_4
Sieghart W, Pinter M, Dauser B, Rohr-Udilova N, Piguet A-C, Prager G, Hayden H, Dienes H-P, Dufour J-F, Peck-Radosavljevic M (2012) Erlotinib and sorafenib in an orthotopic rat model of hepatocellular carcinoma. J Hepatol 57:592–599. https://doi.org/10.1016/j.jhep.2012.04.034
Sung H, Ferlay J, Siegel RL, Laversanne M, Soerjomataram I, Jemal A, Bray F (2021) Global cancer statistics 2020: GLOBOCAN estimates of incidence and mortality worldwide for 36 cancers in 185 countries. CA Cancer J Clin 71:209–249. https://doi.org/10.3322/caac.21660
Tang W, Chen Z, Zhang W, Cheng Y, Zhang B, Wu F, Wang Q, Wang S, Rong D, Reiter FP, De Toni EN, Wang X (2020) The mechanisms of sorafenib resistance in hepatocellular carcinoma: theoretical basis and therapeutic aspects. Signal Transduct Target Ther 5:87. https://doi.org/10.1038/s41392-020-0187-x
Théry C, Amigorena S, Raposo G, Clayton A (2006) Isolation and characterization of exosomes from cell culture supernatants and biological fluids. Curr Protoc Cell Biol. https://doi.org/10.1002/0471143030.cb0322s30

Verma VK, Li H, Wang R, Hirsova P, Mushref M, Liu Y, Cao S, Contreras PC, Malhi H, Kamath PS, Gores GJ, Shah VH (2016) Alcohol stimulates macrophage activation through caspase-dependent hepatocyte derived release of CD40L containing extracellular vesicles. J Hepatol 64:651–660. https://doi.org/10.1016/j.jhep.2015.11.020

Wang Z, Zhao Z, Wu T, Song L, Zhang Y (2015a) Sorafenib-irinotecan sequential therapy augmented the anti-tumor efficacy of monotherapy in hepatocellular carcinoma cells HepG2. Neoplasma 62:172–179. https://doi.org/10.4149/neo_2015_022

Wang Y, Li H, Liang Q, Liu B, Mei X, Ma Y (2015b) Combinatorial immunotherapy of sorafenib and blockade of programmed death-ligand 1 induces effective natural killer cell responses against hepatocellular carcinoma. Tumour Biol 36:1561–1566. https://doi.org/10.1007/s13277-014-2722-2

Wang F, Li L, Piontek K, Sakaguchi M, Selaru FM (2018a) Exosome miR-335 as a novel therapeutic strategy in hepatocellular carcinoma. Hepatology 67:940–954. https://doi.org/10.1002/hep.29586

Wang S, Xu M, Li X, Su X, Xiao X, Keating A, Zhao RC (2018b) Exosomes released by hepatocarcinoma cells endow adipocytes with tumor-promoting properties. J Hematol Oncol 11:82. https://doi.org/10.1186/s13045-018-0625-1

Wang X, Xiang Z, Liu Y, Huang C, Pei Y, Wang X, Zhi H, Wong WH-S, Wei H, Ng IO-L, Lee PP-W, Chan GC-F, Lau Y-L, Tu W (2020) Exosomes derived from Vδ2-T cells control Epstein-Barr virus-associated tumors and induce T cell antitumor immunity. Sci Transl Med. 12:eaaz3426. https://doi.org/10.1126/scitranslmed.aaz3426

Wang Y-T, Cai M-D, Sun L-L, Hua R-N (2021a) A rapid and facile separation-detection integrated strategy for exosome profiling based on boronic acid-directed coupling immunoaffinity. Anal Chem 93:16059–16067. https://doi.org/10.1021/acs.analchem.1c03643

Wang J, Chen D, Ho EA (2021b) Challenges in the development and establishment of exosome-based drug delivery systems. J Control Release 329:894–906. https://doi.org/10.1016/j.jconrel.2020.10.020

Wang X, Zhang Y, Mu X, Tu CR, Chung Y, Tsao SW, Chan GC-F, Leung W-H, Lau Y-L, Liu Y, Tu W (2022) Exosomes derived from γδ-T cells synergize with radiotherapy and preserve antitumor activities against nasopharyngeal carcinoma in immunosuppressive microenvironment. J Immunother Cancer 10:e003832. https://doi.org/10.1136/jitc-2021-003832

Wilhelm SM, Carter C, Tang L, Wilkie D, McNabola A, Rong H, Chen C, Zhang X, Vincent P, McHugh M, Cao Y, Shujath J, Gawlak S, Eveleigh D, Rowley B, Liu L, Adnane L, Lynch M, Auclair D, Taylor I, Gedrich R, Voznesensky A, Riedl B, Post LE, Bollag G, Trail PA (2004) BAY 43–9006 exhibits broad spectrum oral antitumor activity and targets the RAF/MEK/ERK pathway and receptor tyrosine kinases involved in tumor progression and angiogenesis. Cancer Res 64:7099–7109. https://doi.org/10.1158/0008-5472.CAN-04-1443

Witwer KW, Buzás EI, Bemis LT, Bora A, Lässer C, Lötvall J, Nolte-'t Hoen EN, Piper MG, Sivaraman S, Skog J, Théry C, Wauben MH, Hochberg F (2013) Standardization of sample collection, isolation and analysis methods in extracellular vesicle research. J Extracell Vesicles. https://doi.org/10.3402/jev.v2i0.20360

Wu J-Y, Li Y-J, Hu X-B, Huang S, Xiang D-X (2021) Preservation of small extracellular vesicles for functional analysis and therapeutic applications: a comparative evaluation of storage conditions. Drug Deliv 28:162–170. https://doi.org/10.1080/10717544.2020.1869866

Xia S, Pan Y, Liang Y, Xu J, Cai X (2020) The microenvironmental and metabolic aspects of sorafenib resistance in hepatocellular carcinoma. EBioMedicine 51:102610. https://doi.org/10.1016/j.ebiom.2019.102610

Xia C, Dong X, Li H, Cao M, Sun D, He S, Yang F, Yan X, Zhang S, Li N, Chen W (2022) Cancer statistics in China and United States, 2022: profiles, trends, and determinants. Chin Med J (engl) 135:584–590. https://doi.org/10.1097/CM9.0000000000002108

Xiao W, Dong W, Zhang C, Saren G, Geng P, Zhao H, Li Q, Zhu J, Li G, Zhang S, Ye M (2013) Effects of the epigenetic drug MS-275 on the release and function of exosome-related immune molecules in hepatocellular carcinoma cells. Eur J Med Res 18:61. https://doi.org/10.1186/2047-783X-18-61

Xie Z, Gao Y, Ho C, Li L, Jin C, Wang X, Zou C, Mao Y, Wang X, Li Q, Fu D, Zhang Y-F (2022) Exosome-delivered CD44v6/C1QBP complex drives pancreatic cancer liver metastasis by promoting fibrotic liver microenvironment. Gut 71:568–579. https://doi.org/10.1136/gutjnl-2020-323014

Xin H, Li Y, Chopp M (2014) Exosomes/miRNAs as mediating cell-based therapy of stroke. Front Cell Neurosci 8:377. https://doi.org/10.3389/fncel.2014.00377

Xu J, Wan Z, Tang M, Lin Z, Jiang S, Ji L, Gorshkov K, Mao Q, Xia S, Cen D, Zheng J, Liang X, Cai X (2020) N6-methyladenosine-modified CircRNA-SORE sustains sorafenib resistance in hepatocellular carcinoma by regulating β-catenin signaling. Mol Cancer 19:163. https://doi.org/10.1186/s12943-020-01281-8

Xu H, Liao C, Liang S, Ye B-C (2021) A novel peptide-equipped exosomes platform for delivery of antisense oligonucleotides. ACS Appl Mater Interfaces 13:10760–10767. https://doi.org/10.1021/acsami.1c00016

Xue F, Liu Y, Chu H, Wen Y, Yan L, Tang Q, Xiao E, Zhang D, Zhang H (2016) eIF5A2 is an alternative pathway for cell proliferation in cetuximab-treated epithelial hepatocellular carcinoma. Am J Transl Res 8:4670–4681

Ye L, Mayerle J, Ziesch A, Reiter FP, Gerbes AL, De Toni EN (2019) The PI3K inhibitor copanlisib synergizes with sorafenib to induce cell death in hepatocellular carcinoma. Cell Death Discov 5:86. https://doi.org/10.1038/s41420-019-0165-7

Zhang Q, Dehaini D, Zhang Y, Zhou J, Chen X, Zhang L, Fang RH, Gao W, Zhang L (2018) Neutrophil membrane-coated nanoparticles inhibit synovial inflammation and alleviate joint damage in inflammatory arthritis. Nat Nanotechnol 13:1182–1190. https://doi.org/10.1038/s41565-018-0254-4

Zhang R, Gao X, Zuo J, Hu B, Yang J, Zhao J, Chen J (2020) STMN1 upregulation mediates hepatocellular carcinoma and hepatic stellate cell crosstalk to aggravate cancer by triggering the MET pathway. Cancer Sci 111:406–417. https://doi.org/10.1111/cas.14262

Zhao F, Sun X, Lu W, Xu L, Shi J, Yang S, Zhou M, Su F, Lin F, Cao F (2020) Synthesis of novel, DNA binding heterocyclic dehydroabietylamine derivatives as potential antiproliferative and apoptosis-inducing agents. Drug Deliv 27:216–227. https://doi.org/10.1080/10717544.2020.1716879

Zhou Y, Ren H, Dai B, Li J, Shang L, Huang J, Shi X (2018) Hepatocellular carcinoma-derived exosomal miRNA-21 contributes to tumor progression by converting hepatocyte stellate cells to cancer-associated fibroblasts. J Exp Clin Cancer Res 37:324. https://doi.org/10.1186/s13046-018-0965-2

Zhu AX, Rosmorduc O, Evans TRJ, Ross PJ, Santoro A, Carrilho FJ, Bruix J, Qin S, Thuluvath PJ, Llovet JM, Leberre M-A, Jensen M, Meinhardt G, Kang Y-K (2015) SEARCH: a phase III, randomized, double-blind, placebo-controlled trial of sorafenib plus erlotinib in patients with advanced hepatocellular carcinoma. J Clin Oncol 33:559–566. https://doi.org/10.1200/JCO.2013.53.7746

Zhu Y-J, Zheng B, Wang H-Y, Chen L (2017) New knowledge of the mechanisms of sorafenib resistance in liver cancer. Acta Pharmacol Sin 38:614–622. https://doi.org/10.1038/aps.2017.5

Zhu G-Q, Tang Z, Huang R, Qu W-F, Fang Y, Yang R, Tao C-Y, Gao J, Wu X-L, Sun H-X, Zhou Y-F, Song S-S, Ding Z-B, Dai Z, Zhou J, Ye D, Wu D-J, Liu W-R, Fan J, Shi Y-H (2023) CD36+ cancer-associated fibroblasts provide immunosuppressive microenvironment for hepatocellular carcinoma via secretion of macrophage migration inhibitory factor. Cell Discov 9:25. https://doi.org/10.1038/s41421-023-00529-z

Zou S, Tong Q, Liu B, Huang W, Tian Y, Fu X (2020) Targeting STAT3 in cancer immunotherapy. Mol Cancer 19:145. https://doi.org/10.1186/s12943-020-01258-7

Publisher's Note